JPET Fast Forward. Published on March 20, 2020 as DOI: 10.1124/jpet.120.264994
This article has not been copyedited and formatted. The final version may differ from this version.

Title Page

Mechanistic PBPK Modeling of Urine pH Effect on Renal and Systemic Disposition of Methamphetamine and Amphetamine

Weize Huang, Lindsay C. Czuba, Nina Isoherranen

Department of Pharmaceutics, School of Pharmacy, University of Washington, Seattle, WA, 98195

JPET Fast Forward. Published on March 20, 2020 as DOI: 10.1124/jpet.120.264994
This article has not been copyedited and formatted. The final version may differ from this version.

Running Title Page

Running title: PBPK modeling of urine pH effect

Corresponding author: Nina Isoherranen

Address: Health Science Building, Room H-272M, Box 357610, Seattle, WA, 98195-7610

Telephone number: (206) 543-2517

Fax number: (206) 543-3204

Email address: ni2@uw.edu

The number of text pages: 27

The number of tables: 1

The number of figures: 9

The number of words in the Abstract: 250

The number of words in the Introduction: 744

The number of words in the Discussion: 1458

Recommended section assignment: Metabolism, Transport, and Pharmacogenomics

Abbreviations:

AAFE, absolute average fold error

Amph, S(+)-amphetamine

AUC, area under the plasma drug concentration versus time curve

B/P, blood-to-plasma ratio

CL, total plasma clearance

CL_f, formation clearance of the metabolite

CL_{int}, intrinsic clearance for the drug

$CL_{int,m}$, intrinsic clearance for the metabolite

CL_r, renal clearance

CYP2D6, Cytochrome P450 2D6 enzyme

DDI, drug-drug interaction

f_e, fraction elimination of kidney

$f_{u,p}$, unbound fraction in plasma

k_a, absorption constant

K_p, tissue-to-plasma partition coefficient for the drug

$K_{p,m}$, tissue-to-plasma partition coefficient for the metabolite

Meth, S(+)-methamphetamine

MDCK, Madin-Darby canine kidney

PBPK, physiologically-based pharmacokinetics

PET, positron emission tomography

PK, pharmacokinetics

V_{ss}, volume of distribution at steady state

JPET Fast Forward. Published on March 20, 2020 as DOI: 10.1124/jpet.120.264994
This article has not been copyedited and formatted. The final version may differ from this version.

Abstract

The effect of urine pH on renal drug excretion and systemic drug disposition has been observed for many drugs. When urine pH is altered, tubular drug ionization, passive reabsorption, renal clearance, and systemic exposure may all change dramatically, raising clinically significant concerns. Surprisingly, the urine pH effect on drug disposition is not routinely explored in humans, and regulatory agencies have neither developed guidance on this issue nor required industry to conduct pertinent human trials. In this study, we hypothesized that PBPK modeling can be used as a cost-effective method to examine potential urine pH effect on drug and metabolite disposition. Our previously developed and verified mechanistic kidney model was integrated with a full body PBPK model to simulate renal clearance and systemic AUC with varying urine pH statuses, using methamphetamine and amphetamine as model compounds. We first developed and verified drug models for methamphetamine and amphetamine under normal urine pH condition (absolute-average-fold-error (AAFE) < 1.25 at study level). Then, acidic and alkaline urine scenarios were simulated. Our simulation results show that the renal excretion and plasma concentration-time profiles for methamphetamine and amphetamine could be recapitulated under different urine pH (AAFE < 2 at individual level). The methamphetamine-amphetamine parent-metabolite full body PBPK model also successfully simulated amphetamine plasma concentration-time profile (AAFE < 1.25 at study level) and amphetamine/methamphetamine urinary concentration ratio (AAFE < 2 at individual level) after dosing methamphetamine. This demonstrates that our mechanistic PBPK model can predict urine pH effect on systemic and urinary disposition of drugs and metabolites.

JPET Fast Forward. Published on March 20, 2020 as DOI: 10.1124/jpet.120.264994
This article has not been copyedited and formatted. The final version may differ from this version.

Significance Statement

Our study shows that integrating mechanistic kidney model with full body PBPK model can predict the magnitude of alteration in renal excretion and systemic AUC of drugs when urine pH is changed. This provides a cost-effective method to evaluate the likelihood of renal and systemic disposition changes due to varying urine pH. This is important as multiple drugs and diseases can alter urine pH, leading to quantitatively and clinically significant changes in drug and metabolite disposition that may require adjustment of therapy.

Introduction

The effect of urine pH on renal clearance of weak acids and bases was discovered more than half a century ago in studies with salicylic acid (Macpherson *et al.*, 1955) and methamphetamine (Beckett and Rowland, 1965c). The mechanism behind this phenomenon is believed to be the altered ionization status of weak acids and bases with changes in renal tubular filtrate pH, and the subsequent alterations in renal passive reabsorption of unionized drugs (Milne *et al.*, 1958; Tucker, 1981). Changes in renal passive reabsorption can have a drastic impact on renal clearance. For example, when urine pH decreased from alkaline (pH ≈ 7.5-8.5) to acidic (pH ≈ 4.5-5.5), the amount of drug excreted unchanged in urine for weak bases such as pethidine, methamphetamine, and mexiletine increased up to 21-fold (Chan, 1979), 48-fold (Beckett and Rowland, 1965c), and 87-fold (Kiddie *et al.*, 1974), respectively, while the renal clearance of weak acids such as chlorpropamide (Neuvonen and Kärkkäinen, 1983) and salicylic acid (Macpherson *et al.*, 1955) decreased by 99% and 97%, respectively. Also, after dosing of imipramine, methamphetamine, and amitriptyline, their respective metabolites desipramine, amphetamine, and nortriptyline have been shown up to 5-fold (Gram *et al.*, 1971), 11-fold (Beckett and Rowland, 1965b), and 93-fold (Kärkkäinen and Neuvonen, 1986) increases in urinary excretion, respectively, in acidic urine condition in comparison to alkaline urine condition. These findings demonstrate the pronounced and broad significance of the urine pH effect on both drugs and metabolites.

Overall, approximately 31% of marketed drugs are significantly excreted unchanged via the kidney (Varma *et al.*, 2009), and 70% of marketed drugs are either monoprotic weak acids or monoprotic weak bases (Manallack, 2007) that may have varying ionization statuses in the tubular lumen. In addition, the mean logP of patented compounds across 18 pharmaceutical companies ranged from 3.5 to 4.5 (Leeson and St-Gallay, 2011), suggesting that the majority of drugs have a moderate to

high intrinsic lipophilicity and therefore transcellular permeability. Together, these data suggest that many drugs are potentially subject to significant renal clearance and effective renal passive reabsorption that can be altered due to urine pH changes. As such, the variability of renal clearance with urine pH can be surprisingly common. Indeed, more than a dozen drugs have been shown to have urine pH-dependent renal excretion (Macpherson *et al.*, 1955; Beckett and Rowland, 1965a; c; Sharpstone, 1969; Sjöqvist *et al.*, 1969; Gerhardt *et al.*, 1969; Gram *et al.*, 1971; Kiddie *et al.*, 1974; Chan, 1979; Neuvonen and Kärkkäinen, 1983; Muhiddin *et al.*, 1984; Benowitz and Jacob, 1985; Aoki and Sitar, 1988; Freudenthaler *et al.*, 1998). If renal excretion is an important elimination pathway for the drug of interest, the systemic drug disposition will also be affected by altered urine pH. For example, for weak bases memantine and flecainide, the area under the plasma drug concentration-time curve ($AUC_{0\text{-}inf}$) increased by 5.3-fold (Freudenthaler *et al.*, 1998) and 3.6-fold (Muhiddin *et al.*, 1984), respectively, while for weak acids cinoxacin and chlorpropamide, the plasma $AUC_{0\text{-}inf}$ decreased by 67% (Barbhaiya *et al.*, 1982) and 81% (Neuvonen and Kärkkäinen, 1983), respectively, in alkaline urine condition in comparison to acidic urine condition. This demonstrates that the magnitude of urine pH effect on plasma AUC could be as significant as drug-drug interactions resulting from co-administration with a strong inhibitor or inducer (i.e. AUC increased by 5-fold or decreased by 80%).

Given the number of known drugs affected by urine pH and the substantial magnitude of observed urine pH effects on drug and metabolite disposition, it is striking that urine pH effects on drug and metabolite renal and systemic disposition are not routinely examined for weak acids and bases in clinical studies, and regulatory agencies have not developed guidelines to assess drug safety under different urine pHs. In contrast, characterization of drug-drug interactions, food effects and disease effects on drug disposition are required by regulatory agencies as essential components of drug

approval process, and these interactions and effects have been explored extensively in human subjects and simulated by models (Shebley *et al.*, 2018) to support regulatory decision making.

In this study, we hypothesized that modeling techniques could be leveraged to understand and predict urine pH effect on drug and metabolite disposition. To test this hypothesis, a recently developed and verified dynamic physiologically-based mechanistic kidney model (Huang and Isoherranen, 2018) was integrated into a parent-metabolite full body physiologically based pharmacokinetic (PBPK) model (Huang and Isoherranen, 2020) to simulate urine pH dependent parent-metabolite systemic disposition and urinary excretion using methamphetamine and amphetamine as model compounds.

Materials and Methods

Development of parent-metabolite full body physiologically based pharmacokinetic (PBPK) structural model with mechanistic kidney model and peripheral arm vein sampling site

A 104-compartment parent-metabolite (52 compartments for each) full-body PBPK model was developed using MATLAB and Simulink platform (R2018a; MathWorks, Natick, MA) by merging our previously published mechanistic kidney model (Huang and Isoherranen, 2018) with the parent-metabolite full-body PBPK model (Huang and Isoherranen, 2020), as shown in Figure 1. This model contains ten physiologically important tissue/organ compartments modeled as perfusion-rate limited organs, two blood circulation compartments (i.e. central venous compartment and central arterial compartment), a peripheral arm vein sampling site as previously described (Huang and Isoherranen, 2020), a 2-compartment permeability-rate limited liver model, and a 35-compartment mechanistic kidney model (Huang and Isoherranen, 2018). The mechanistic kidney model was incorporated to replace the conventional perfusion-rate limited kidney compartment, to capture the unbound filtration, active secretion, and tubular filtrate/urine pH-dependent passive reabsorption. The mechanistic kidney model was merged with the PBPK model by connecting the central arterial compartment to the glomerulus to create the renal inflow and connecting the vascular compartment of the last subsegment of collecting duct to the central venous compartment to create the renal outflow. The model file and the code script are provided as Supplementary Material.

JPET Fast Forward. Published on March 20, 2020 as DOI: 10.1124/jpet.120.264994
This article has not been copyedited and formatted. The final version may differ from this version.

Physicochemical parameters for methamphetamine and amphetamine

In this study, only dextrorotary isomers of methamphetamine and amphetamine (i.e. S(+)-methamphetamine and S(+)-amphetamine) are discussed due to their greater psychoactive activity compared to the levorotatory isomers. The molecular weight, pK_a, and LogP values of methamphetamine (Meth) and amphetamine (Amph) were collected from www.drugbank.ca. The plasma unbound fractions ($f_{u,p}$) of methamphetamine and amphetamine were determined in pooled human plasma by ultracentrifugation as previously described (Shirasaka *et al.*, 2013). In brief, pooled human plasma was spiked with methamphetamine and amphetamine to a final concentration of 0.2 µM. Three 200 µL aliquots were centrifuged in 435,000 g for 90 min at 37 °C and another three 200 µL aliquots were incubated at 37 °C for 90 min. The supernatant (50 µL) from the ultracentrifugation and the incubated samples (50 µL) were then quenched with 250 µL of 3:1 (v/v) acetonitrile:methanol containing 100 nM methamphetamine-d_{11} and amphetamine-d_{11} as internal standards and analyzed by LC-MS/MS as previously described (Wagner *et al.*, 2017). The experiments were conducted in triplicate on two separate days. The plasma unbound fraction for each day was calculated as the ratio of mean free concentration (C_u) in supernatant (after ultracentrifugation) over mean total concentration (C) in plasma (after incubation). The average value of the two experiments was used as the final plasma unbound fraction ($f_{u,p}$).

The blood-to-plasma ratio (B/P) of methamphetamine and amphetamine were experimentally determined as described previously (Sager *et al.*, 2016). Methamphetamine and amphetamine were spiked into 3 mL of fresh human blood to a final concentration of 0.2 µM. Three 700 µL aliquots were collected and incubated for 2 hours at 37 °C to equilibrate blood partitioning. Blood samples (60 µL) were collected after incubation to measure blood concentration, remaining samples were centrifuged in 1,000 g for 10 min to separate plasma and a plasma sample (60 µL) was collected

JPET Fast Forward. Published on March 20, 2020 as DOI: 10.1124/jpet.120.264994
This article has not been copyedited and formatted. The final version may differ from this version.

to measure plasma concentration. Both blood and plasma samples (60 µL) were then quenched with 120 µL of methanol containing 100 nM methamphetamine-d_{11} and amphetamine-d_{11} as internal standards and analyzed by LC-MS/MS as previously described (Wagner *et al.*, 2017). The experiments were conducted in triplicate on two separate days and the blood-to-plasma ratio was calculated as the ratio of concentration in blood sample over concentration in plasma sample. The average value of the two experiments was used as the final blood-to-plasma ratio.

The cellular permeabilities of methamphetamine and amphetamine were measured using Madin-Darby canine kidney (MDCK) cells (ATCC CCL-34 passage 10 to 15). The cells were cultured in Dulbecco's modified Eagle's medium (DMEM) supplemented with 10% fetal bovine serum (FBS), 4.5 g/L glucose, and 1% penicillin/streptomycin, at 37°C with 5% CO_2 in a humidified atmosphere. Cells were seeded at a density of approximately 6.5×10^4 cells/cm^2 on 24-well Transwell plates with 0.4 µm pore size inserts. Ninety-six hours after seeding, cells were used for permeability assays. For the preincubation, the apical and basolateral chambers were first rinsed twice with warm Hank's Balanced Salt Solution (HBSS) pH 7.2, followed by acclimation to HBSS for 15 minutes. Membrane integrity was confirmed by transepithelial electrical resistance (TEER) measurements and monolayers with values below 200 Ω×cm^2 were excluded from the study. Transport assay was initiated by replacing the buffer on either apical or basolateral side with test solutions (200 µL apical, 800 µL basolateral donor chambers) containing 1 µM of methamphetamine or amphetamine in HBSS (pH 7.2). Samples of 100 µL medium from the receiver chamber were collected at 0, 20, 40, 60, 90, and 120 minutes for analysis by LC-MS/MS using a previously published method (Wagner *et al.*, 2017). The apparent permeability (P_{app}) of methamphetamine and amphetamine across cell monolayers was calculated using eq. 1:

$$P_{app} = \frac{dQ/dt}{A\times C_0} \quad (1)$$

JPET Fast Forward. Published on March 20, 2020 as DOI: 10.1124/jpet.120.264994
This article has not been copyedited and formatted. The final version may differ from this version.

where A is the membrane surface area (cm^2) of the insert filter, C_0 is the initial concentration of compound in the donor chamber (μM), and dQ/dt (μmol/s) is the slope of the linear regression line of measured drug amount in receiver chamber (Q) as a function of time (t), and represents the amount of methamphetamine or amphetamine that crossed the monolayer per unit time. The experiments were conducted for both apical-to-basolateral (A-to-B) and basolateral-to-apical (B-to-A) directions in duplicates on three separate days. The average value of P_{app} measured in both directions in three experiments was used as the final apparent permeability. Detailed results are shown in Supplementary Figures 1 and 2.

PBPK model development for methamphetamine and amphetamine

The overall workflow for model development and verification is shown in Figure 2. For the drug model development, the clinical pharmacokinetic data of methamphetamine and amphetamine in humans were collected from the National Center for Biotechnology Information database (http://www.ncbi.nlm.nih.gov/pubmed) accessed on January 1st, 2019. Search keywords were "methamphetamine OR amphetamine AND pharmacokinetics". One iv (Li *et al.*, 2010) and two po (Rowland, 1969; CDER, 2001) datasets were used as training sets for methamphetamine and amphetamine model development, respectively. Seven (six iv and one po) and two (both po) datasets published in 6 studies (Perez-Reyes *et al.*, 1991; Cook *et al.*, 1993; Mendelson *et al.*, 1995, 2006; CDER, 2002; Harris *et al.*, 2003) were used as test sets to verify the developed PBPK models for methamphetamine and amphetamine, respectively. The detailed information of study populations and study designs for all the datasets used are summarized in Supplementary Table 1. Plasma concentration-time curves and urinary excretion profiles from these studies were digitized using WebPlotDigitizer (version 4.2, https://automeris.io/WebPlotDigitizer).

JPET Fast Forward. Published on March 20, 2020 as DOI: 10.1124/jpet.120.264994
This article has not been copyedited and formatted. The final version may differ from this version.

For oral drug absorption of both methamphetamine and amphetamine, compounds in the gastrointestinal lumen were assumed to be completely dissolved and evenly distributed inside the lumen compartment immediately upon oral administration. The drug absorption from lumen into intestinal blood was assumed to be governed by a single absorption rate constant k_a, which was set to be a sufficiently high value such that the overall absorption was intestinal blood flow limited. This was based on the high aqueous solubility (928 mg/L and 1740 mg/L (www.drugbank.ca)) and high permeability of methamphetamine and amphetamine. The gut metabolism of methamphetamine and amphetamine was assumed to be negligible as both drugs have low extraction ratios in the liver primarily mediated by CYP2D6, and CYP2D6 is not highly expressed in the intestine (Paine *et al.*, 2006). As such, the fraction absorbed (F_a) and fraction escaping gut clearance (F_g) were assumed to be 1.

For the physiological model, the system-specific parameters including the physical volume and the blood flow to each organ/tissue were collected from literature (Brown *et al.*, 1997). The tissue-to-plasma partition coefficients (K_p) for brain, gastrointestinal tract, heart, kidney, liver, lung, pancreas, and spleen for methamphetamine were calculated based on a published human positron emission tomography (PET) study (Volkow *et al.*, 2010), while the K_p values for adipose, bone, muscle, and skin were optimized as K_p=3 based on observed methamphetamine volume of distribution at steady state (V_{ss}) of 4.02 L/kg (Harris *et al.*, 2003). Due to the structural similarity between methamphetamine and amphetamine, the visceral organ-specific K_p values (i.e. K_p for brain, gastrointestinal tract, heart, kidney, liver, lung, pancreas, and spleen) for amphetamine were set the same as methamphetamine. Based on the higher polarity of amphetamine in comparison to methamphetamine, the tissue-specific K_p values of adipose, bone, muscle, and skin were set as 2

for amphetamine, resulting in a predicted V_{ss} of 3.14 L/kg, versus an observed apparent V_{ss} ranging from 3.2 L/kg to 5.6 L/kg after oral dosing (Randall, 2004).

The hepatic clearances of methamphetamine and amphetamine were modeled based on *in vivo* human data. Methamphetamine has an observed systemic clearance of 18.0 L/hr (Li *et al.*, 2010) and an observed renal clearance of 8.09 L/hr (Li *et al.*, 2010) after intravenous administration. Amphetamine has an observed oral clearance of 15.8 L/hr (CDER, 2001) and an observed renal clearance of 7.14 L/hr (Rowland, 1969). As a result, the hepatic clearances of methamphetamine and amphetamine were calculated as 9.91 L/hr and 7.41 L/hr, respectively, based on the assumption that F_a and F_g are equal to 1 for amphetamine. The intrinsic metabolic clearances of methamphetamine and amphetamine were back-calculated as 14.4 and 9.87 L/hr respectively based on measured plasma unbound fraction, blood-to-plasma ratio, and the well-stirred hepatic clearance model (Wilkinson and Shand, 1975).

The mechanistic kidney model was used to simulate the renal clearance of methamphetamine and amphetamine. The experimentally determined human plasma unbound fraction ($f_{u,p}$) and the permeability in the MDCK cells were used as model inputs to simulate unbound filtration and passive reabsorption processes as previously described (Huang and Isoherranen, 2018). Without incorporating active secretion, the mechanistic kidney model predicted CL_r values of 2.9 L/hr and 3.2 L/hr for methamphetamine and amphetamine, respectively, which are significantly below the observed values (8.09 L/hr for methamphetamine (Li *et al.*, 2010) and 7.14 L/hr for amphetamine (Rowland, 1969)). Therefore, an active secretion component was added to the mechanistic kidney model to simulate methamphetamine and amphetamine renal clearances based on the previous characterization of methamphetamine and amphetamine as OCT2 and MATE substrates (Wagner *et al.*, 2017). Due to the low confidence of *in vitro* and *in vivo* renal transporter quantification and

expression, the active secretion clearances of methamphetamine and amphetamine were optimized with respect to the observed renal clearance (i.e. 8.09 L/hr for methamphetamine (Li *et al.*, 2010) and 7.14 L/hr for amphetamine (Rowland, 1969)) assuming equal apical and basolateral secretion and uniform distribution of active secretion among the three subsegments of proximal tubule in the model. All the detailed physicochemical and pharmacokinetic values used in the models are listed in Table 1.

Verification of methamphetamine and amphetamine PBPK models

All simulations were performed using MATLAB and Simulink platform (R2018a; MathWorks, Natick, MA) with the same route of administration and the same dosage regimen as reported in the corresponding clinical studies (Supplementary Table 1), assuming a representative population with average physiology. The renal tubular filtrate pH gradient for a representative population is shown in Supplementary Table 2 with a urine pH value of 6.5 under uncontrolled (i.e. normal) condition. The overall model development and verification workflow was adapted from previous studies (Huang *et al.*, 2017; Cheong *et al.*, 2019), and is shown schematically in Figure 2. To verify the methamphetamine model, methamphetamine plasma concentration-time profiles were simulated after intravenous and oral dosing and compared to the observed data from 7 test sets (6 iv and 1 po dosing) published in 5 studies (Perez-Reyes *et al.*, 1991; Cook *et al.*, 1993; Mendelson *et al.*, 1995, 2006; Harris *et al.*, 2003). These studies were not used in model development. For amphetamine model verification, the amphetamine plasma concentration-time profiles were simulated after oral dosing and compared to the observed data from 2 test datasets (CDER, 2002) that were not used in model development. All simulated plasma concentrations were sampled from peripheral arm vein sampling site which was developed and verified previously (Huang and

Isoherranen, 2020) to match with the sampling site in the observed PK studies. To assess model performance, absolute average fold error (AAFE) was calculated according to equation 2. Furthermore, the area under the simulated plasma concentration-time curve (AUC) was calculated using trapezoidal method and compared to the observed AUC. The ratio between the simulated and observed AUC was calculated to assess the fold-difference between the two. The calculated AAFE and AUC ratio had to be within 0.8-to-1.25-fold (model acceptance criterion) for the simulation to be considered successful.

$$AAFE = 10^{\frac{1}{n}\sum\left|log_{10}\frac{Simulated}{Observed}\right|} \quad (2)$$

Simulation and verification of urine pH effect on renal excretion and systemic disposition of methamphetamine and amphetamine

To evaluate whether the verified full body PBPK model could be applied to predict urine pH effect on plasma concentration-time profile and urinary drug excretion of methamphetamine and amphetamine, methamphetamine disposition was simulated under two different urine pH conditions in contrast to the default uncontrolled urine pH (i.e. urine pH = 6.5). For acidic urine pH, the tubular filtrate pH was set to decrease in a stepwise manner from 7.2 at the first proximal tubule subsegment to 5.0 at the last collecting duct subsegment. For alkaline urine pH, the tubular filtrate pH was set to increase in a stepwise manner from 7.4 at the first proximal tubule subsegment to 8.0 at the last collecting duct subsegment. Detailed renal tubular filtrate pH gradient setups used in the modeling are shown in Supplementary Table 2.

The amount of drug excreted in urine with time and the plasma concentration-time profile for methamphetamine were simulated at each of the three urine pH conditions after oral dosing of 11 mg methamphetamine base. The simulated urinary excretion versus time profiles were compared

to observed data from three test sets corresponding to the three urine pH conditions (Beckett and Rowland, 1965c). Due to the limited number of subjects in the observed data (n=1), a 2-fold acceptance criterion of AAFE was used as the acceptance criterion when the simulated population representative was compared to the individual observed data. The 2-fold criterion was selected given the reported inter-individual variability (coefficient of variance: 56%) in methamphetamine renal clearance (Kim *et al.*, 2004). The 2-fold range is a conservative criterion provided renal clearance follows log-normal distribution, where 95% of individuals have a renal clearance within 2.53-19.5 L/hr, yielding a 2.77-fold difference between the upper/lower limit and the geometric mean. The simulation results of the urine pH effect on methamphetamine urinary excretion were also compared to another clinical study (Beckett and Rowland, 1965b) as a second set of verification. Because the observed plasma concentration-time data for methamphetamine were not available under the basic and acidic urine pH conditions, simulated and observed plasma concentrations were not compared.

The urinary excretion and plasma concentration-time profile for amphetamine were simulated similarly under uncontrolled, acidic, and alkaline urine conditions after oral dosing of 11 mg amphetamine base. The percentage of amphetamine dose excreted into urine was calculated by dividing the cumulative amount excreted into urine by dose. The amount excreted into urine was considered over 48 hours for uncontrolled urine pH and 16 hours for acidic and alkaline urine pH as described in the observed study, and compared to observed data from respective test datasets (Beckett and Rowland, 1965a). The effect of altered urine pH on amphetamine urinary excretion was evaluated based on the percent change in urinary excretion (amount of amphetamine excreted) under either acidic or alkaline urine in comparison to the urinary excretion when urine pH was not controlled (simulated urine pH = 6.5). The ratio of the predicted to observed percent change in

urinary excretion with altered urine pH was calculated. A 2-fold acceptance criterion, similar to what has been used for drug-drug interaction studies (Sager *et al.*, 2015), was applied to this ratio to determine whether the simulation was successful. Additionally, simulated plasma concentration-time profile for amphetamine under uncontrolled and acidic urine conditions was compared to the observed data from four test datasets (Beckett *et al.*, 1969). Due to the limited number of subjects in the observed data (n=2), a 2-fold acceptance criterion of AAFE was used when comparing the simulated population mean results to the individual observed data.

Verification of methamphetamine-amphetamine parent-metabolite model

The methamphetamine-amphetamine parent-metabolite model was established based on the individual compound models using previously developed PBPK model (Huang and Isoherranen, 2020). Amphetamine formation from methamphetamine was modeled to occur within the liver compartment. The hepatic formation clearance of amphetamine from methamphetamine was calculated as 3.29 L/hr using the data from a clinical study reporting the AUC ratio of amphetamine to methamphetamine (ratio = 0.208) after iv dosing of methamphetamine (Newton *et al.*, 2005) and observed amphetamine oral clearance of 15.8 L/hr (CDER, 2001) based on a previous method (Lane and Levy, 1980).

To verify the methamphetamine-amphetamine parent-metabolite kinetic model, amphetamine plasma concentration-time profiles as a metabolite of methamphetamine after intravenous administration of methamphetamine were simulated and compared to the observed data from 4 test sets (Cook *et al.*, 1993; Harris *et al.*, 2003; Mendelson *et al.*, 2006). To evaluate the model, a 0.8-to-1.25-fold acceptance criterion was applied to the AAFE to determine whether the simulation was successful. All simulations were performed with the same route of administration and same

dosage as reported in the corresponding studies (Supplementary Table 1) and all simulated plasma concentrations were sampled from the peripheral arm vein sampling site.

To test whether the verified parent-metabolite model can capture the methamphetamine-amphetamine urinary kinetics under different urine pH conditions, simulation results were compared to observed urinary concentration ratio (Oyler *et al.*, 2002) and excretion data (Kim *et al.*, 2004). First, the urinary concentration of methamphetamine and amphetamine were simulated under uncontrolled urine pH (urine pH = 6.5) after 4 consecutive oral doses of 10 or 20 mg methamphetamine. The urinary metabolite/parent concentration ratio was calculated as the ratio of amphetamine to methamphetamine urinary concentration, and the ratio was compared to the observed data (Oyler *et al.*, 2002). Since the observed data were reported only from a single subject after 10 or 20 mg doses, a 2-fold acceptance criterion for the calculated AAFE was used to determine whether the simulation was successful. For extrapolation, we also simulated the urinary metabolite/parent concentration ratio under acidic and alkaline urine conditions. As the observed urinary metabolite/parent ratio data were not available under the acidic and alkaline urine pH conditions, no comparisons between simulated and observed urinary concentrations were done for these two conditions. Second, the amount of methamphetamine and amphetamine excreted in urine was simulated under uncontrolled urine pH (urine pH = 6.5) after 4 consecutive doses of 10 mg methamphetamine. The percentage of methamphetamine dose excreted into urine as methamphetamine or amphetamine was calculated by dividing cumulative amount of methamphetamine and amphetamine excreted into urine over 16 days by methamphetamine dose. The urinary metabolite/parent excretion ratio was calculated by dividing the urinary excretion of amphetamine with the urinary excretion of methamphetamine. The simulated percentage of

urinary excretion of methamphetamine and amphetamine, and the metabolite/parent ratio were compared to observed data from 13 individuals (Kim *et al.*, 2004).

Results

Development and verification of methamphetamine and amphetamine drug models

Human plasma unbound fraction, blood-to-plasma ratio, and MDCK cellular permeability were experimentally determined for methamphetamine and amphetamine and used in the PBPK model. The $f_{u,p}$ value was 0.77 (±0.03) for methamphetamine and 0.82 (±0.09) for amphetamine. The blood-to-plasma ratio was 1.04 (±0.07) for methamphetamine and 1.04 (±0.06) for amphetamine, suggesting some distribution into the red blood cells. The MDCK cellular permeability was 29.1×10^{-6} (±5.75) cm/s for methamphetamine and 26.9×10^{-6} (±4.42) cm/s for amphetamine (Supplementary Figures 1 and 2), indicating a high permeability for both compounds.

The methamphetamine (Figure 3) and amphetamine (Figure 4) drug models were independently verified using the observed plasma concentration-time data from seven methamphetamine test sets (six iv dosing and one oral dosing) (Perez-Reyes *et al.*, 1991; Cook *et al.*, 1993; Mendelson *et al.*, 1995, 2006; Harris *et al.*, 2003) and two amphetamine oral dosing test sets (CDER, 2002), respectively. The AAFE values for methamphetamine (Figure 3) and amphetamine (Figure 4) plasma concentration-time data in the test sets ranged from 1.04 to 1.19 and the predicted over observed AUC ratios ranged from 0.87 to 1.11 (Supplementary Table 1 and Supplementary Figure 3). A plot showing the relationship between predicted and observed concentrations for the simulated studies is also shown in Supplementary Figure 3. Both evaluation metrics met the stringent 0.8-to-1.25-fold model acceptance criterion demonstrating successful model verification and high confidence on the model parameter inputs for both methamphetamine and amphetamine.

Simulation and verification of urine pH effect on renal excretion and systemic disposition of methamphetamine and amphetamine

After the successful verification of the methamphetamine systemic model, methamphetamine urinary excretion was simulated as a function of time under different urine pH conditions. The goal of these simulations was to test whether the effect of urine pH on methamphetamine excretion could be simulated using the full body PBPK model coupled with the mechanistic kidney model. Our simulations show that methamphetamine urinary excretion when urine is acidic (Figure 5a red dashed curve) significantly exceeds the excretion when urine is alkaline (Figure 5a blue dotted curve), and that the simulated urinary excretion profile of methamphetamine under alkaline or acidic urine agrees with the observed data in human (Beckett and Rowland, 1965c). The simulated excretion of methamphetamine with urine pH of 6.5 (Figure 5a black solid curve) is in between the acidic and alkaline urine conditions (Figure 5a red and blue). The urine pH of 6.5 was selected to represent the estimated urine pH in individuals when urine pH is not controlled. The calculated AAFE values met the 2-fold model acceptance criterion under all three urine pH conditions (Figure 5a). The urine pH effect on urinary excretion was also simulated and compared to a second observed study, shown in Supplementary Figure 4. The percent dose excreted in urine as methamphetamine was successfully captured under all three urine pH conditions, with all calculated AAFE values meeting the 2-fold model acceptance criterion (Supplementary Figure 4). The urine pH effect on methamphetamine systemic disposition was also simulated (Figure 5b) to explore the effect of changes in urine pH on methamphetamine exposure and half-life. The calculated plasma methamphetamine $AUC_{0\text{-}inf}$ values under alkaline, uncontrolled, and acidic urine conditions were 970, 542, and 284 μg×hr/L, respectively, after an oral dose of 11 mg methamphetamine base, illustrating a dramatic impact of urine pH on methamphetamine systemic

exposure. The simulated plasma concentrations of methamphetamine were highest when urine was alkaline, followed by uncontrolled urine pH (urine pH = 6.5), and the plasma concentrations of methamphetamine were the lowest when urine was acidic (Figure 5b).

Similar to methamphetamine, urine pH also plays a significant role in amphetamine urinary excretion (Beckett and Rowland, 1965a). To recapitulate the urine pH effect on amphetamine renal disposition, the urinary excretion of amphetamine was simulated under three different urine pH conditions (Figure 6a). Compared to uncontrolled urine pH condition (urine pH = 6.5), alkaline urine condition was predicted to result in a 97% decrease of urinary excretion of amphetamine, while the observed decrease was 91%, resulting in a predicted over observed ratio of 1.07-fold meeting the acceptance criterion of 2-fold. On the other hand, urine acidification was predicted to result in a 48% increase of urinary excretion of amphetamine when compared to uncontrolled urine pH condition, while the observed increase was 75%, resulting in a predicted over observed ratio of 0.64-fold meeting the acceptance criterion of 2-fold.

The urine pH effect on amphetamine systemic disposition was also simulated (Figure 6b and 6c) and compared to the observed data (Beckett *et al.*, 1969). The AAFE values for the simulations of acidic and uncontrolled urine pH met the 2-fold model acceptance criterion (Figure 6b and 6c). The 2-fold criterion was used due to the small sample size in the observed studies (n=2). Unfortunately, clinical data regarding the alkaline urine pH effect on amphetamine systemic disposition were not available, and hence no verification was conducted for this condition. Based on the simulations using the verified amphetamine model, the plasma amphetamine $AUC_{0\text{-}inf}$ values under alkaline, uncontrolled, and acidic urine conditions were 1325, 692, and 361 μg×hr/L, respectively, after an oral dose of 11 mg amphetamine base, demonstrating a dramatic impact of urine pH on amphetamine systemic exposure.

JPET Fast Forward. Published on March 20, 2020 as DOI: 10.1124/jpet.120.264994
This article has not been copyedited and formatted. The final version may differ from this version.

Simulation and verification of plasma and urinary methamphetamine-amphetamine parent-metabolite kinetics

After the successful verification of methamphetamine (Figure 3) and amphetamine (Figure 4) models, the parent-metabolite link was established to allow for simulation of amphetamine disposition as a metabolite of methamphetamine. To verify the methamphetamine-amphetamine parent-metabolite model, amphetamine plasma concentration-time profiles were simulated as a metabolite after iv dosing of methamphetamine and compared to observed data. As shown in Figure 7, all AAFE values were within the 0.8-to-1.25-fold acceptance criterion, indicating the parent-metabolite linkage between methamphetamine and amphetamine was successfully established and verified.

To evaluate the applicability of the verified parent-metabolite model to capture the methamphetamine-amphetamine urinary kinetics, the urinary metabolite/parent concentration ratio was simulated under uncontrolled urine pH (urine pH=6.5) and compared to the observed data (Oyler *et al.*, 2002) from a single subject after 4 consecutive doses of 10 mg or 20 mg methamphetamine (Figure 8). The AAFE values for these simulations were within the 2-fold acceptance criterion, which was used due to the small sample size (n=1). The urinary metabolite/parent concentration ratio was also simulated under acidic and alkaline urine conditions to explore the impact of varying urine pH on this measure. The simulation results show that the urinary metabolite/parent concentration ratio can be affected by urine pH. Particularly, alkaline urine resulted in a higher urinary Amph/Meth ratio. In addition, the percent dose excreted in urine as methamphetamine and amphetamine was also simulated under uncontrolled urine pH (urine pH = 6.5) and compared to the observed data (Figure 9). The observed mean percent dose excreted in

urine as methamphetamine and amphetamine were 41.3% and 9.8%, respectively, while the predicted values were 40.6% and 8.2% respectively. The observed amphetamine/methamphetamine ratio in urine was 0.26 while the predicted ratio was 0.20. The predicted/observed values were all within the 2-fold acceptance criterion. Together, these data suggest successful application of the model to simulate systemic and urinary parent-metabolite kinetics.

Discussion

The effect of urine pH on renal excretion of drugs has been observed for a multitude of drugs in humans (Macpherson *et al.*, 1955; Beckett and Rowland, 1965a; c; Sharpstone, 1969; Sjöqvist *et al.*, 1969; Gerhardt *et al.*, 1969; Gram *et al.*, 1971; Kiddie *et al.*, 1974; Chan, 1979; Muhiddin *et al.*, 1984; Benowitz and Jacob, 1985; Aoki and Sitar, 1988; Freudenthaler *et al.*, 1998). In addition, a plethora of medications and disease states have been reported to cause changes in urine pH (Cook *et al.*, 2007). For example, acetazolamide which was indicated for glaucoma and edema has been shown to increase urinary pH in humans from 5.5 to 7.6 (Moviat *et al.*, 2006). In contrast, cholestyramine, indicated for hypercholesterolemia, was shown to induce metabolic acidosis and therefore can decrease urinary pH to as low as 4.8 (Eaves and Korman, 1984). Further, urine acidification is observed with diabetes, obesity, and chronic kidney disease (Maalouf *et al.*, 2004, 2010; Nakanishi *et al.*, 2012), and urine alkalinization is observed with vomiting and urinary tract infection (Yi *et al.*, 2012; Lai *et al.*, 2019). Therefore, the potential impact of co-medications and comorbidities on urine pH and consequently renal drug clearance can be commonplace and profound. Nonetheless, the overall effect of altered urine pH on urinary drug concentrations, excretion profiles, systemic exposure, and the subsequent clinical consequences has been underappreciated. In this study, we hypothesized that *in silico* modeling could be used to understand and predict the effects of altered urine pH on drug and metabolite renal and systemic disposition. The goal of this study was to integrate the verified mechanistic kidney model (Huang and Isoherranen, 2018) with a parent-metabolite full body PBPK model (Huang and Isoherranen, 2020) to examine the applicability of the final model to predict the effect of varying urine pH on renal clearance and systemic exposure to assess the potential clinical consequences, using methamphetamine and amphetamine as model compounds.

JPET Fast Forward. Published on March 20, 2020 as DOI: 10.1124/jpet.120.264994
This article has not been copyedited and formatted. The final version may differ from this version.

Currently, the urine pH effect on renal clearance and systemic disposition have rarely been considered when using *in silico* techniques to simulate drug and metabolite disposition. For studies that specifically explore urinary excretion as a function of time, the urinary excretion profiles were mostly simulated using simple first order urinary kinetics (Ortiz *et al.*, 2014; Phillips *et al.*, 2014; Adachi *et al.*, 2015; Marchand *et al.*, 2015; Yang *et al.*, 2015) governed by a fixed observed value such as elimination rate constant. Although these models may have successfully recapitulated the observed data, they cannot be extrapolated to untested or altered scenarios due to their non-mechanistic nature when simulating urinary kinetics. In contrast, mechanistic modeling can be used to extrapolate drug disposition from known settings to unstudied scenarios such as unstudied populations and unstudied drug co-administration (Wagner *et al.*, 2015; Huang *et al.*, 2017; Zhang *et al.*, 2017; Hanke *et al.*, 2018), and likely to unstudied urine pH conditions.

Recently, the MechKiM model embedded in the Simcyp platform was used to predict renal clearance and urine pH effects on renal clearance (Matsuzaki *et al.*, 2019). In that study, seven compounds were used as the test set to examine model performance, and the simulations were conducted assuming uniform renal tubular filtrate pH throughout all renal segments. The overall simulation results under the uncontrolled urine pH condition showed AAFE values ranging from 2.87 (assuming uniform tubular filtrate pH = 6.2) to 3.62 (assuming uniform tubular filtrate pH = 7.4). In comparison, our mechanistic kidney model which assumes a tubular pH gradient across different tubular segments showed superior performance for a set of 35 non-neutral test compounds with AAFE values of 1.83, 1.82, and 1.46 for weak bases, weak acids, and zwitterions, respectively (Huang and Isoherranen, 2018). This better performance could be due to our strategy to use a stepwise gradient for renal tubular filtrate pH to account for the naturally continuous acidification process of tubular filtrate, although other differences such as microvilli consideration and a larger

number (11 vs 7) of tubular compartments in our model may also contribute to our better performance. Further, the previous study (Matsuzaki *et al.*, 2019) showed a relatively insensitive response of simulated renal clearance to urine pH changes. For example, their simulated amphetamine renal clearance did not change with urine pH between 5 and 8, which is inconsistent with the observed dramatic changes (Beckett and Rowland, 1965a; Beckett *et al.*, 1969). Conversely, our model accurately recapitulated the renal excretion of methamphetamine and amphetamine under acidic (urine pH = 5.0), uncontrolled (urine pH = 6.5), and alkaline (urine pH = 8.0) urine conditions (Figure 6), and was previously shown to capture the varying renal clearance of salicylic acid and memantine as a function of urine pH (Huang and Isoherranen, 2018). We confirmed the importance of the stepwise gradient via an in-house head-to-head comparison of the urinary methamphetamine excretion using our stepwise pH gradients and the previously published (Matsuzaki *et al.*, 2019) constant pH value. The constant pH value approach failed to recapitulate the observed data under uncontrolled (AAFE = 2.2 or 6.5) and alkaline urine condition (AAFE = 13.6) (Supplementary Figure 5) while the stepwise pH gradient approach successfully (AAFE < 2) simulated methamphetamine urinary excretion (Supplementary Figure 4). Together, these results support that our PBPK model and strategy can capture the mathematical relationship between urine pH and the corresponding apparent permeability, passive reabsorption, and renal clearance successfully. More examination using additional dataset is warranted for further validation of the full model.

Altered urine pH may also affect the systemic exposure of drugs and their metabolites if renal clearance is an important elimination pathway. For example, amphetamine plasma AUC was decreased by approximately 50% under acidic urine pH condition compared to uncontrolled urine pH condition (Beckett *et al.*, 1969), and as urine pH is known to affect the renal clearance for many

drugs, such effects on drug AUC can be common. The modeling and simulation workflow presented here offers a feasible approach to predict whether the drug exposure is sensitive to changes in urine pH. To do this, it is important to construct both urine pH-sensitive mechanistic kidney model and a full body PBPK model that captures drug absorption, distribution, and other pathways of elimination such as hepatic metabolism and biliary excretion. In this study, we first verified the full body PBPK model for methamphetamine (Figure 3) and amphetamine (Figure 4), and then verified the urine pH effect on renal excretion (Figure 5a and 6a), to ultimately simulate the urine pH effect on plasma AUC for methamphetamine (Figure 5b) and amphetamine (Figure 6b and 6c). Based on the simulations, we also predicted that urine alkalinization can increase plasma AUC of methamphetamine and amphetamine by about 100% in comparison to uncontrolled urine pH due to increased passive reabsorption and decreased renal clearance (Figures 5 and 6). Collectively, we showed a modeling workflow that can serve as a robust and cost-effective method to assess how drug AUC is altered when urine pH is changed due to co-medications or disease states.

The urine pH effect also impacts the interpretation of urinary concentration data. At present, the urinary concentrations of drugs and metabolites have been widely used for understanding drug pharmacokinetics, for phenotyping human subjects for certain metabolizing enzymes (Wedlund *et al.*, 1984; Chládek *et al.*, 2000; Vogl *et al.*, 2015), and for testing and screening for illicit drug use (Fabbri, 2003; Moeller *et al.*, 2017). As shown in Figures 5 and 6, the changes in urine pH will change the renal excretion and therefore urinary concentration-time profile. Further, simulations in Figure 8 suggest that urinary metabolite/parent ratio can also be influenced by urine pH changes. Currently, urine samples collected at a single time point often serve as the direct proxy for data interpretation, without the quantitative consideration of the confounding effect of different urine

pHs on urinary disposition. As such, analysis of drug concentrations in the collected urine samples may lead to misinterpretation and suboptimal decision making. The modeling and simulation approach described here, together with the measurement of urine pH values, can aid in interpreting urinary excretion data and help to minimize false negative and false positive readings.

In conclusion, this study shows that the previously developed and verified mechanistic kidney model together with the full body parent-metabolite PBPK model can accurately predict the effect of urine pH on methamphetamine and amphetamine renal clearance, plasma concentration-time profile and systemic and urinary parent-metabolite kinetics. These results suggest that mechanistic PBPK models can be generally applied to predict the potential impact of co-medications and comorbidities on parent-metabolite renal and systemic disposition due to altered urine pH. The modeling workflow and approach established here is likely to be useful in assessing the sensitivity of new compounds' disposition to changes in urine pH, especially for weak acids and bases that have substantial permeability.

Acknowledgements:

The authors would like to thank Dr. David J. Wagner for his skillful assistance in preliminary permeability experiments.

Authorship Contributions:

Participated in research design: Huang, Czuba, and Isoherranen

Conducted experiments: Huang and Czuba

Performed data analysis: Huang, Czuba, and Isoherranen

Wrote or contributed to the writing of the manuscript: Huang, Czuba, and Isoherranen

Reference

Adachi K, Suemizu H, Murayama N, Shimizu M, and Yamazaki H (2015) Human biofluid concentrations of mono(2-ethylhexyl)phthalate extrapolated from pharmacokinetics in chimeric mice with humanized liver administered with di(2-ethylhexyl)phthalate and physiologically based pharmacokinetic modeling. *Environ Toxicol Pharmacol* **39**:1067–1073, Elsevier B.V.

Aoki FY, and Sitar DS (1988) Clinical pharmacokinetics of amantadine hydrochloride. *Clin Pharmacokinet* **14**:35–51.

Barbhaiya RH, Gerber AU, Craig WA, and Welling PG (1982) Influence of urinary pH on the pharmacokinetics of cinoxacin in humans and on antibacterial activity in vitro. *Antimicrob Agents Chemother* **21**:472–480.

Beckett AH, and Rowland M (1965a) Urinary excretion kinetics of amphetamine in man. *J Pharm Pharmacol* **17**:628–39.

Beckett AH, and Rowland M (1965b) Urinary excretion kinetics of methylamphetamine in man. *J Pharm Pharmacol* **17**:109S-114S.

Beckett AH, and Rowland M (1965c) Urinary excretion of methylamphetamine in man. *Nature* **206**:1260–1261.

Beckett AH, Salmon JA, and Mitchard M (1969) The relation between blood levels and urinary excretion of amphetamine under controlled acidic and under fluctuating urinary pH values using [14C] amphetamine. *J Pharm Pharmacol* **21**:251–8.

Benowitz NL, and Jacob P (1985) Nicotine renal excretion rate influences nicotine intake during

cigarette smoking. *J Pharmacol Exp Ther* **234**:153–5.

Brown RP, Delp MD, Lindstedt SL, Rhomberg LR, and Beliles RP (1997) Physiological parameter values for physiologically based pharmacokinetic models. *Toxicol Ind Health* **13**:407–84.

CDER (2002) Application number 11-522. Clinical Pharmacology and biopharmaceutics review(s).

CDER (2001) Application number 21-303. Clinical Pharmacology and biopharmaceutics review(s).

Chan K (1979) The effects of physiocochemical properties of pethidine and its basic metabolites on their buccal absorption and renal elimination. *J Pharm Pharmacol* **31**:672–5.

Cheong EJY, Teo DWX, Chua DXY, and Chan ECY (2019) Systematic Development and Verification of A Physiologically-Based Pharmacokinetic Model of Rivaroxaban. *Drug Metab Dispos* dmd.119.086918.

Chládek J, Zimová G, Beránek M, and Martínková J (2000) In-vivo indices of CYP2D6 activity: Comparison of dextromethorphan metabolic ratios in 4-h urine and 3-h plasma. *Eur J Clin Pharmacol* **56**:651–657.

Collins KP, Jackson KM, and Gustafson DL (2018) Hydroxychloroquine: A Physiologically-Based Pharmacokinetic Model in the Context of Cancer-Related Autophagy Modulation. *J Pharmacol Exp Ther* jpet.117.245639.

Cook CE, Jeffcoat AR, Hill JM, Pugh DE, Patetta PK, Sadler BM, White WR, and Perez-Reyes M (1993) Pharmacokinetics of methamphetamine self-administered to human subjects by

smoking S-(+)-methamphetamine hydrochloride. *Drug Metab Dispos* **21**:717–23.

Cook JD, Strauss KA, Caplan YH, LoDico CP, and Bush DM (2007) Urine pH: The effects of time and temperature after collection. *J Anal Toxicol* **31**:486–496.

Dubbelboer IR, Lilienberg E, Sjögren E, and Lennernäs H (2017) A Model-Based Approach To Assessing the Importance of Intracellular Binding Sites in Doxorubicin Disposition. *Mol Pharm* **14**:686–698.

Eaves ER, and Korman MG (1984) Cholestyramine induced hyperchloremic metabolic acidosis. *Aust N Z J Med* **14**:670–2.

Emond C, Sanders JM, Wikoff D, and Birnbaum LS (2013) Proposed mechanistic description of dose-dependent BDE-47 urinary elimination in mice using a physiologically based pharmacokinetic model. *Toxicol Appl Pharmacol* **273**:335–344, Elsevier Inc.

Fabbri A (2003) Comprehensive drug screening in decision making of patients attending the emergency department for suspected drug overdose. *Emerg Med J* **20**:25–28.

Freudenthaler S, Meineke I, Schreeb KH, Boakye E, Gundert-Remy U, and Gleiter CH (1998) Influence of urine pH and urinary flow on the renal excretion of memantine. *Br J Clin Pharmacol* **46**:541–546.

Gerhardt RE, Knouss RF, Thyrum PT, Luchi RJ, and Morris JJ (1969) Quinidine excretion in aciduria and alkaluria. *Ann Intern Med* **71**:927–33.

Gram LF, Kofod B, Christiansen J, and Rafaelsen OJ (1971) Imipramine metabolism: PH-Dependent distribution and urinary excretion. *Clin Pharmacol Ther* **12**:239–244.

Hanke N, Frechen S, Moj D, Britz H, Eissing T, Wendl T, and Lehr T (2018) PBPK Models for

CYP3A4 and P-gp DDI Prediction: A Modeling Network of Rifampicin, Itraconazole, Clarithromycin, Midazolam, Alfentanil, and Digoxin. *CPT pharmacometrics Syst Pharmacol* **7**:647–659.

Harris DS, Boxenbaum H, Everhart ET, Sequeira G, Mendelson JE, and Jones RT (2003) The bioavailability of intranasal and smoked methamphetamine. *Clin Pharmacol Ther* **74**:475–486.

Huang W, and Isoherranen N (2018) Development of a Dynamic Physiologically Based Mechanistic Kidney Model to Predict Renal Clearance. *CPT Pharmacometrics Syst Pharmacol* **7**:593–602.

Huang W, and Isoherranen N (2020) Sampling Site Has a Critical Impact on Physiologically Based Pharmacokinetic Modeling. *J Pharmacol Exp Ther* **372**:30–45.

Huang W, Nakano M, Sager J, Ragueneau-Majlessi I, and Isoherranen N (2017) Physiologically Based Pharmacokinetic Model of the CYP2D6 Probe Atomoxetine: Extrapolation to Special Populations and Drug-Drug Interactions. *Drug Metab Dispos* **45**:1156–1165.

Kärkkäinen S, and Neuvonen PJ (1986) Pharmacokinetics of amitriptyline influenced by oral charcoal and urine pH. *Int J Clin Pharmacol Ther Toxicol* **24**:326–32.

Kiddie MA, Kaye CM, Turner P, and Shaw TR (1974) The influence of urinary pH on the elimination of mexiletine. *Br J Clin Pharmacol* **1**:229–32.

Kim I, Oyler JM, Moolchan ET, Cone EJ, and Huesitis MA (2004) Urinary pharmacokinetics of methamphetamine and its metabolite, amphetamine following controlled oral administration to humans. *Ther Drug Monit* **26**:664–672.

Lai HC, Chang SN, Lin HC, Hsu YL, Wei HM, Kuo CC, Hwang KP, and Chiang HY (2019) Association between urine pH and common uropathogens in children with urinary tract infections. *J Microbiol Immunol Infect*, doi: 10.1016/j.jmii.2019.08.002, Elsevier Taiwan LLC.

Lane EA, and Levy RH (1980) Prediction of steady-state behavior of metabolite from dosing of parent drug. *J Pharm Sci* **69**:610–2.

Leeson PD, and St-Gallay SA (2011) The influence of the "organizational factor" on compound quality in drug discovery. *Nat Rev Drug Discov* **10**:749–765, Nature Publishing Group.

Li L, Everhart T, Jacob P, Jones R, and Mendelson J (2010) Stereoselectivity in the human metabolism of methamphetamine. *Br J Clin Pharmacol* **69**:187–192.

Maalouf NM, Cameron MA, Moe OW, and Sakhaee K (2010) Metabolic basis for low urine pH in type 2 diabetes. *Clin J Am Soc Nephrol* **5**:1277–1281.

Maalouf NM, Sakhaee K, Parks JH, Coe FL, Adams-Huet B, and Pak CYC (2004) Association of urinary pH with body weight in nephrolithiasis. *Kidney Int* **65**:1422–1425.

Macpherson CR, Milne MD, and Evans BM (1955) The excretion of salicylate. *Br J Pharmacol Chemother* **10**:484–9.

Manallack DT (2007) The pK(a) Distribution of Drugs: Application to Drug Discovery. *Perspect Medicin Chem* **1**:25–38.

Marchand A, Aranda-Rodriguez R, Tardif R, Nong A, and Haddad S (2015) Human inhalation exposures to toluene, ethylbenzene, and m-xylene and physiologically based pharmacokinetic modeling of exposure biomarkers in exhaled air, blood, and urine. *Toxicol*

Sci **144**:414–424.

Matsuzaki T, Scotcher D, Darwich AS, Galetin A, and Rostami-Hodjegan A (2019) Towards Further Verification of Physiologically-Based Kidney Models: Predictability of the Effects of Urine-Flow and Urine-pH on Renal Clearance. *J Pharmacol Exp Ther* **368**:157–168.

Mendelson J, Jones RT, and Upton R (1995) Methamphetamine in humans and ethanol interactions. *Clin Pharmacol Ther* **57**:559–568.

Mendelson J, Uemura N, Harris D, Nath RP, Fernandez E, Jacob P, Everhart ET, and Jones RT (2006) Human pharmacology of the methamphetamine stereoisomers. *Clin Pharmacol Ther* **80**:403–420.

Milne MD, Scribner BH, and Crawford MA (1958) Non-ionic diffusion and the excretion of weak acids and bases. *Am J Med* **24**:709–29.

Moeller KE, Kissack JC, Atayee RS, and Lee KC (2017) Clinical Interpretation of Urine Drug Tests. *Mayo Clin Proc* **92**:774–796, Mayo Foundation for Medical Education and Research.

Moviat M, Pickkers P, van der Voort PHJ, and van der Hoeven JG (2006) Acetazolamide-mediated decrease in strong ion difference accounts for the correction of metabolic alkalosis in critically ill patients. *Crit Care* **10**.

Muhiddin KA, Johnston A, and Turner P (1984) The influence of urinary pH on flecainide excretion and its serum pharmacokinetics. *Br J Clin Pharmacol* **17**:447–51.

Nakanishi N, Fukui M, Tanaka M, Toda H, Imai S, Yamazaki M, Hasegawa G, Oda Y, and Nakamura N (2012) Low urine pH is a predictor of chronic kidney disease. *Kidney Blood Press Res* **35**:77–81.

Neuvonen PJ, and Kärkkäinen S (1983) Effects of charcoal, sodium bicarbonate, and ammonium chloride on chlorpropamide kinetics. *Clin Pharmacol Ther* **33**:386–93.

Newton TF, Roache JD, De La Garza R 2nd, Fong T, Wallace CL, Li S-H, Elkashef A, Chiang N, Kahn R, T.F. N, J.D. R, R. DLGII, T. F, C.L. W, S.-H. L, A. E, and N. C (2005) Safety of intravenous methamphetamine administration during treatment with bupropion. *Psychopharmacology (Berl)* **182**:426–435.

Ortiz RH, Maître A, Barbeau D, Lafontaine M, and Bouchard M (2014) Use of physiologically-based pharmacokinetic modeling to simulate the profiles of 3-hydroxybenzo(a)pyrene in workers exposed to polycyclic aromatic hydrocarbons. *PLoS One* **9**.

Oyler JM, Cone EJ, Joseph RE, Moolchan ET, and Huestis MA (2002) Duration of detectable methamphetamine and amphetamine excretion in urine after controlled oral administration of methamphetamine to humans. *Clin Chem* **48**:1703–14.

Paine MF, Hart HL, Ludington SS, Haining RL, Rettie AE, and Zeldin DC (2006) The human intestinal cytochrome P450 "pie." *Drug Metab Dispos* **34**:880–886.

Pang KS, Sun H, Liu L, Yang QJ, Fan J, and Chen S (2016) Metabolite Kinetics: The Segregated Flow Model for Intestinal and Whole Body Physiologically Based Pharmacokinetic Modeling to Describe Intestinal and Hepatic Glucuronidation of Morphine in Rats In Vivo. *Drug Metab Dispos* **44**:1123–1138.

Perez-Reyes M, White WR, McDonald SA, Hicks RE, Jeffcoat AR, Hill JM, and Cook CE (1991) Clinical effects of daily methamphetamine administration. *Clin Neuropharmacol* **14**:352–8.

Phillips MB, Yoon M, Young B, and Tan Y-M (2014) Analysis of biomarker utility using a PBPK/PD model for carbaryl. *Front Pharmacol* **5**:1–10.

Randall B (2004) *Disposition of toxic drugs and chemicals in man, seven edition*.

Rowland M (1969) Amphetamine blood and urine levels in man. *J Pharm Sci* **58**:508–9.

Sager JE, Price LSL, and Isoherranen N (2016) Stereoselective Metabolism of Bupropion to OH-bupropion, Threohydrobupropion, Erythrohydrobupropion, and 4'-OH-bupropion in vitro. *Drug Metab Dispos* **44**:1709–19.

Sager JE, Yu J, Ragueneau-Majlessi I, and Isoherranen N (2015) Physiologically Based Pharmacokinetic (PBPK) Modeling and Simulation Approaches: A Systematic Review of Published Models, Applications, and Model Verification. *Drug Metab Dispos* **43**:1823–37.

Sharpstone P (1969) The renal handling of trimethoprim and sulphamethoxazole in man. *Postgrad Med J* **45**:Suppl:38-42.

Shebley M, Sandhu P, Emami Riedmaier A, Jamei M, Narayanan R, Patel A, Peters SA, Reddy VP, Zheng M, de Zwart L, Beneton M, Bouzom F, Chen J, Chen Y, Cleary Y, Collins C, Dickinson GL, Djebli N, Einolf HJ, Gardner I, Huth F, Kazmi F, Khalil F, Lin J, Odinecs A, Patel C, Rong H, Schuck E, Sharma P, Wu SP, Xu Y, Yamazaki S, Yoshida K, and Rowland M (2018) Physiologically Based Pharmacokinetic Model Qualification and Reporting Procedures for Regulatory Submissions: A Consortium Perspective. *Clin Pharmacol Ther* **104**:88–110.

Shirasaka Y, Sager JE, Lutz JD, Davis C, and Isoherranen N (2013) Inhibition of CYP2C19 and CYP3A4 by omeprazole metabolites and their contribution to drug-drug interactionss. *Drug*

Metab Dispos **41**:1414–1424.

Sjöqvist F, Berglund F, Borgå O, Hammer W, Andersson S, and Thorstrand C (1969) The pH-dependent excretion of monomethylated tricyclic antidepressants. In dog and man. *Clin Pharmacol Ther* **10**:826–833.

Tucker GT (1981) Measurement of the renal clearance of drugs. *Br J Clin Pharmacol* **12**:761–70.

Varma MVS, Feng B, Obach RS, Troutman MD, Chupka J, Miller HR, and El-Kattan A (2009) Physicochemical determinants of human renal clearance. *J Med Chem* **52**:4844–4852.

Vogl S, Lutz RW, Schönfelder G, and Lutz WK (2015) CYP2C9 genotype vs. metabolic phenotype for individual drug dosing-A correlation analysis using flurbiprofen as probe drug. *PLoS One* **10**.

Volkow ND, Fowler JS, Wang GJ, Shumay E, Telang F, Thanos PK, and Alexoff D (2010) Distribution and pharmacokinetics of methamphetamine in the human body: Clinical implications. *PLoS One* **5**:1–6.

Wagner C, Zhao P, Pan Y, Hsu V, Grillo J, Huang SM, and Sinha V (2015) Application of Physiologically Based Pharmacokinetic (PBPK) Modeling to Support Dose Selection: Report of an FDA Public Workshop on PBPK. *CPT pharmacometrics Syst Pharmacol* **4**:226–30.

Wagner DJ, Sager JE, Duan H, Isoherranen N, and Wang J (2017) Interaction and transport of methamphetamine and its primary metabolites by organic cation and multidrug and toxin extrusion transporters. *Drug Metab Dispos* **45**:770–778.

Wedlund PJ, Aslanian WS, McAllister CB, Wilkinson GR, and Branch RA (1984) Mephenytoin hydroxylation deficiency in Caucasians: frequency of a new oxidative drug metabolism polymorphism. *Clin Pharmacol Ther* **36**:773–780.

Wilkinson GR, and Shand DG (1975) Commentary: a physiological approach to hepatic drug clearance. *Clin Pharmacol Ther* **18**:377–90.

Worley RR, and Fisher J (2015) Application of physiologically-based pharmacokinetic modeling to explore the role of kidney transporters in renal reabsorption of perfluorooctanoic acid in the rat. *Toxicol Appl Pharmacol* **289**:428–441.

Yang X, Doerge DR, Teeguarden JG, and Fisher JW (2015) Development of a physiologically based pharmacokinetic model for assessment of human exposure to bisphenol A. *Toxicol Appl Pharmacol* **289**:442–456, Elsevier B.V.

Yi JH, Han SW, Song JS, and Kim HJ (2012) Metabolic alkalosis from unsuspected ingestion: Use of urine pH and anion Gap. *Am J Kidney Dis* **59**:577–581.

Zhang Z, Imperial MZ, Patilea-Vrana GI, Wedagedera J, Gaohua L, and Unadkat JD (2017) Development of a novel maternal-fetal physiologically based pharmacokinetic model I: Insights into factors that determine fetal drug exposure through simulations and sensitivity analyses. *Drug Metab Dispos* **45**:920–938.

Footnotes:

This work was supported by National Institutes of Health grant P01 DA032507. Weize Huang was supported by Warren G. Magnuson Scholarship and William E. Bradley Fellowship from the University of Washington, Seattle, WA.

JPET Fast Forward. Published on March 20, 2020 as DOI: 10.1124/jpet.120.264994
This article has not been copyedited and formatted. The final version may differ from this version.

Figure Legends

Figure 1. Structure of the developed mechanistic kidney-integrated parent-metabolite full body PBPK model. Schematic presentation of the physiologically based parent-metabolite pharmacokinetic model with a mechanistic kidney model and peripheral arm vein sampling site incorporated. The renal artery that connects central artery to the entrance of the mechanistic kidney model is shown in red dashed lines. The renal vein that connects the exit of mechanistic kidney model to the central venous compartment is shown in blue dashed lines. The transporter-mediated active secretion or active reabsorption is shown in black dotted arrows. The bidirectional pH-dependent passive diffusion is shown in double arrows. The peripheral arm vein sampling sites are shown in orange with forearm anastomoses shown in magenta. The intravenous and oral dosing are shown in green. Q_{kidney}, renal blood flow; Q_{urine}, urine formation flow; GFR, glomerular filtration rate; i, the number of subsegment each segment is divided into.

Figure 2. The overall workflow for developing and verifying the full body parent-metabolite PBPK model of methamphetamine and amphetamine for the simulation of urine pH-dependent systemic disposition and urinary excretion. Meth, methamphetamine. Amph, amphetamine. $f_{u,p}$, unbound fraction in plasma. B/P, blood-to-plasma ratio. MDCK, Madin-Darby canine kidney. P_{app}, experimentally determined apparent cellular permeability. CL_{iv}, total body clearance measured after intravenous dosing. CL_{po}, total body clearance measured after oral dosing. CL_r, renal clearance. PET, positron emission tomography. AAFE, absolute average fold error. M/P, metabolite-to-parent ratio.

Figure 3. Simulation of methamphetamine (Meth) plasma concentration-time profile after iv dosing. Methamphetamine plasma concentration-time profiles were simulated after intravenous dosing and the simulated plasma concentrations (shown in red) were compared to the observed data (shown in blue) from 6 different test sets. The calculated AAFE value for each dataset is shown in each panel. The observed data for methamphetamine are from (a) (Cook *et al.*, 1993), (b) (Mendelson *et al.*, 1995), (c) (Harris *et al.*, 2003), (d) (Harris *et al.*, 2003), (e) (Mendelson *et al.*, 2006), and (f) (Mendelson *et al.*, 2006).

Figure 4. Simulation of methamphetamine (Meth) and amphetamine (Amph) plasma concentration-time profiles after oral dosing. Methamphetamine and amphetamine plasma concentration-time profiles were simulated after oral dosing and the simulated plasma concentrations (red lines) were compared to the observed data (blue circles) from 3 different test sets. The calculated AAFE value for each dataset is shown in each panel. The observed data for methamphetamine (a) are from (Perez-Reyes *et al.*, 1991), and the observed data for amphetamine (b and c) are from (CDER, 2002).

Figure 5. Simulation of the urine pH effect on methamphetamine urinary excretion and plasma concentration-time profile of methamphetamine (Meth). Methamphetamine urinary excretion profiles (a) and plasma concentration-time profiles (b) were simulated after 11 mg methamphetamine oral administration under acidic urine pH condition (red dashed curves), uncontrolled urine pH condition (black solid curves), and alkaline urine pH condition (blue dotted curves). Simulated methamphetamine urinary excretion as a function of time was compared to observed data (N=1) under 3 different urine conditions (Beckett and Rowland, 1965c) shown in

JPET Fast Forward. Published on March 20, 2020 as DOI: 10.1124/jpet.120.264994
This article has not been copyedited and formatted. The final version may differ from this version.

red squares (acidic urine), black circles (uncontrolled pH urine), and blue triangles (alkaline urine). The calculated AAFE values for all three urine conditions are shown in the insets.

Figure 6. Simulation of the effect of urine pH on the urinary excretion and plasma concentration-time profile of amphetamine. Amphetamine urinary excretion over 48 hours (uncontrolled urine pH shown in black), 16 hours (alkaline urine pH shown in blue), and 16 hours (acidic urine pH shown in red) was simulated after 11 mg amphetamine oral administration (a). The observed individual data of amphetamine excretion are shown in circles (Beckett and Rowland, 1965a). The mean simulated amount (as percent of dose) of amphetamine excreted in urine under each urine pH condition is shown in triangles with 2-fold error bars. Simulated (curves) amphetamine plasma concentration-time profiles (b and c) are shown in comparison to the observed (open symbols, (Beckett *et al.*, 1969)) data in two individual subjects under uncontrolled urine pH (black symbols and solid curve), acidic urine pH (red symbols and dashed curve), and alkaline urine pH (blue dotted curve) after 11 mg oral administration of amphetamine. The calculated AAFE values for each individual subject are shown. $AAFE_{un}$ represents the calculated AAFE comparing simulated and observed amphetamine plasma concentrations under uncontrolled urine pH. $AAFE_{acid}$ represents the calculated AAFE comparing simulated and observed amphetamine plasma concentrations under acidic urine pH.

Figure 7. Simulation of plasma amphetamine concentration-time profile as a metabolite after iv dosing of methamphetamine. Amphetamine plasma concentration-time profiles were simulated (shown in red curves) as the metabolite of methamphetamine after iv dosing of methamphetamine and compared to the observed data (shown in blue circles) from 4 test sets. The calculated AAFE values were all within the 0.8-to-1.25-fold range. The observed data of

amphetamine are from (a) (Cook *et al.*, 1993), (b) (Harris *et al.*, 2003), (c) (Mendelson *et al.*, 2006), (d) (Mendelson *et al.*, 2006).

Figure 8. Simulation of the time course of metabolite to parent (amphetamine/methamphetamine) urinary concentration ratio after multiple oral doses of methamphetamine. Amphetamine/methamphetamine urinary ratio was simulated under acidic urine pH condition (red curves), uncontrolled urine pH condition (black curve), and alkaline urine pH condition (blue curve) after 4 consecutive oral doses of methamphetamine and compared to the observed urinary ratio (black circles) from 2 test sets (Oyler *et al.*, 2002) with 10 mg dose (panel a) and 20 mg dose (panel b) under uncontrolled urine pH condition. The calculated AAFE values comparing simulation and observation under uncontrolled urine pH condition are shown in insets.

Figure 9. Simulation of the amount of methamphetamine and its metabolite amphetamine excretion into urine (as a percent of methamphetamine dose) after multiple oral dosing of methamphetamine. Panel (a) shows the simulated fraction (in red square with two-fold error bars) of methamphetamine dose excreted into urine as methamphetamine and amphetamine (expressed as a percent of methamphetamine dose) after 4 oral doses of 10 mg methamphetamine and assuming urine pH of 6.5 to mimic uncontrolled urine pH. The simulated Amph/Meth urinary excretion ratio (in red square with two-fold error bars) based on the data presented in (a) is shown in panel (b). The observed data (Kim *et al.*, 2004) for individual subjects are shown in blue circles and observed means are shown in blue triangles.

JPET Fast Forward. Published on March 20, 2020 as DOI: 10.1124/jpet.120.264994
This article has not been copyedited and formatted. The final version may differ from this version.

Table 1. Physicochemical and pharmacokinetic parameters of methamphetamine and amphetamine used in the full body parent-metabolite PBPK model with the integrated mechanistic kidney model and peripheral arm vein sampling site.

Parameter	Methamphetamine	Amphetamine
Physicochemical		
Molecular weight (g/mol)	149.23[a]	135.21[a]
Compound type	Base[a]	Base[a]
pK_a	10.21[a]	10.01[a]
LogP	2.23[a]	1.85[a]
$f_{u,p}$	0.77[b]	0.82[b]
B/P	1.04[b]	1.04[b]
MDCK cellular permeability (10^{-6} cm/s)	29.1[b]	26.9[b]
Absorption		
k_a (hr^{-1})	5[c]	5[c]
F_a	1[c]	1[c]
F_g	1[c]	1[c]
Distribution		
$K_{p,adipose}$	3[d]	2[d]
$K_{p,bone}$	3[d]	2[d]
$K_{p,brain}$	9.67[e]	9.67[e]
$K_{p,gastrointestinal\ tract}$	25.2[e]	25.2[e]
$K_{p,heart}$	5.21[e]	5.21[e]
$K_{p,kidney}$	14.5[e]	14.5[e]
$K_{p,liver}$	25[e]	25[e]
$K_{p,lung}$	6.94[e]	6.94[e]
$K_{p,muscle}$	3[d]	2[d]
$K_{p,pancreas}$	12.7[e]	12.7[e]
$K_{p,skin}$	3[d]	2[d]
$K_{p,spleen}$	11[e]	11[e]
Metabolism		
CL_{total} (L/hr)	18.0[f] (i.v.)	15.8[g] (p.o.)
CL_h (L/hr)	9.91[h]	7.41[h]
$CL_{intrinsic}$ (L/hr)	14.4[h]	9.87[h]
CL_f (L/hr)	-	3.29[i]
Excretion		
CL_r (L/hr)	8.09[f]	7.14[j]
$CL_{section}$ (L/hr)	48[k] (16×3)	30[k] (10×3)

JPET Fast Forward. Published on March 20, 2020 as DOI: 10.1124/jpet.120.264994
This article has not been copyedited and formatted. The final version may differ from this version.

$f_{u,p}$, fraction unbound in plasma; B/P, blood-to-plasma ratio; MDCK, Madin-Darby canine kidney; k_a, absorption rate constant from gut lumen to blood; F_a, fraction absorbed; F_g, fraction passed the enterocyte; K_p, tissue-to-plasma partition coefficient for specific organ/tissue; CL_{total}, total body clearance (intravenous administration for methamphetamine; oral administration for amphetamine); CL_h, hepatic clearance; $CL_{intrinsic}$, metabolic intrinsic clearance; CL_f, formation clearance; CL_r, renal clearance; $CL_{section}$, renal active secretion clearance at proximal tubule (clearance value of each proximal subsegment S1, S2, and S3) [a]Collected from www.drugbank.ca, [b]Measured from experiments, [c]Assumed as described in Materials and Methods, [d]Optimized as described in Materials and Methods, [e](Volkow *et al.*, 2010), [f](Li *et al.*, 2010), [g](CDER, 2001), [h]Derived as described in Materials and Methods, [i]Derived based on (Lane and Levy, 1980; CDER, 2001; Newton *et al.*, 2005), [j](Rowland, 1969), [k]Optimized as described in Materials and Methods

JPET Fast Forward. Published on March 20, 2020 as DOI: 10.1124/jpet.120.264994
This article has not been copyedited and formatted. The final version may differ from this version.

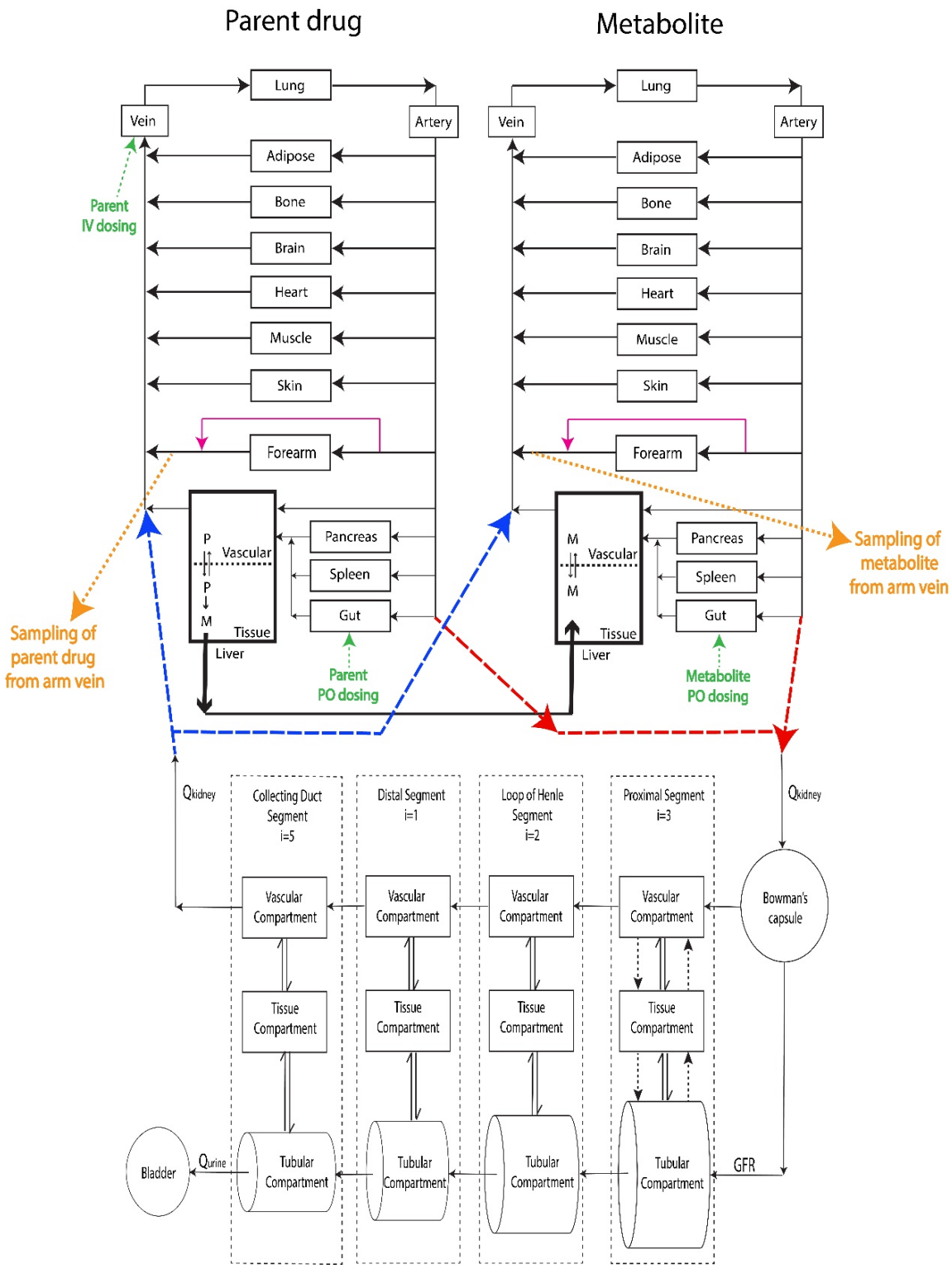

Figure 1.

JPET Fast Forward. Published on March 20, 2020 as DOI: 10.1124/jpet.120.264994
This article has not been copyedited and formatted. The final version may differ from this version.

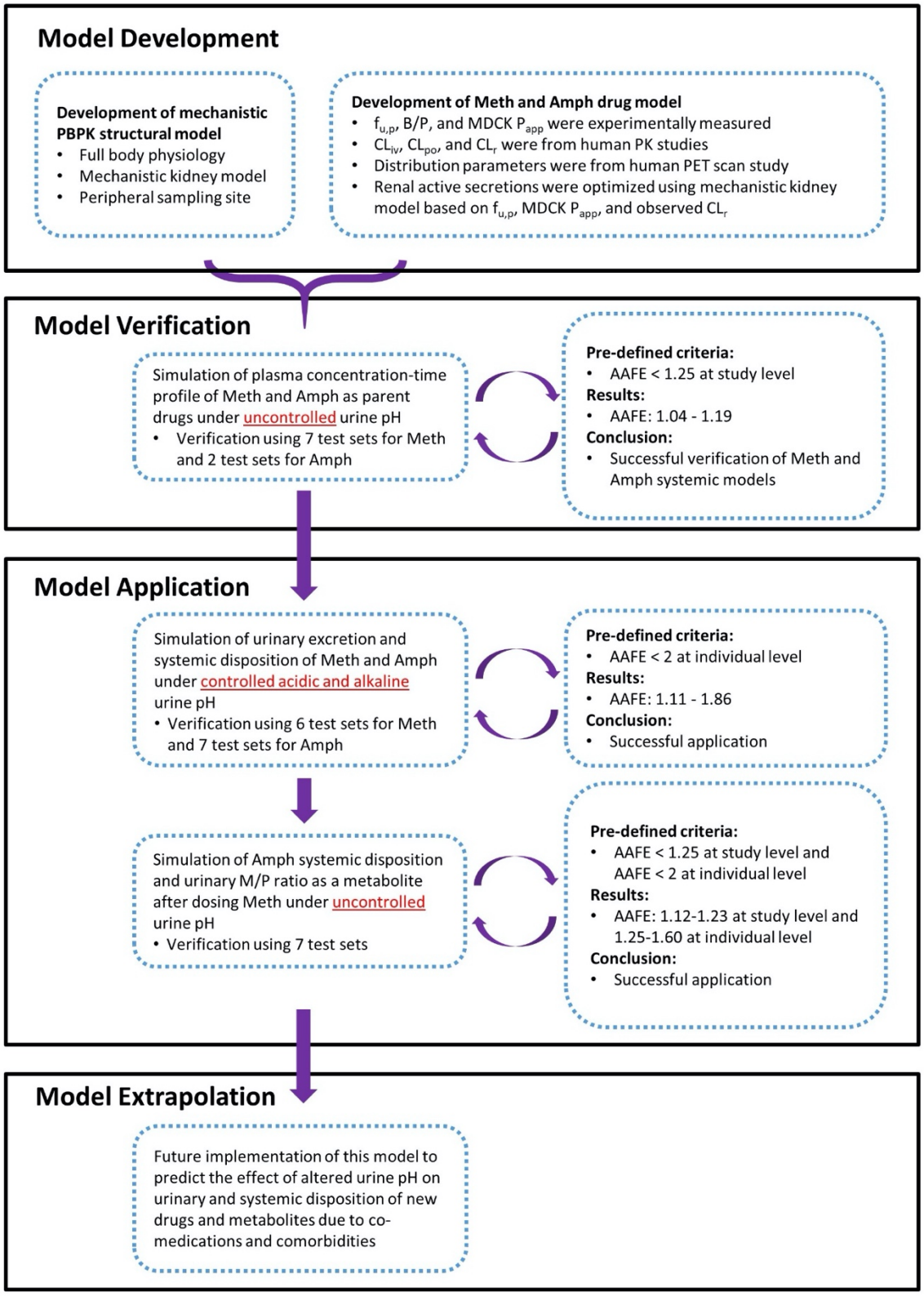

Figure 2.

JPET Fast Forward. Published on March 20, 2020 as DOI: 10.1124/jpet.120.264994
This article has not been copyedited and formatted. The final version may differ from this version.

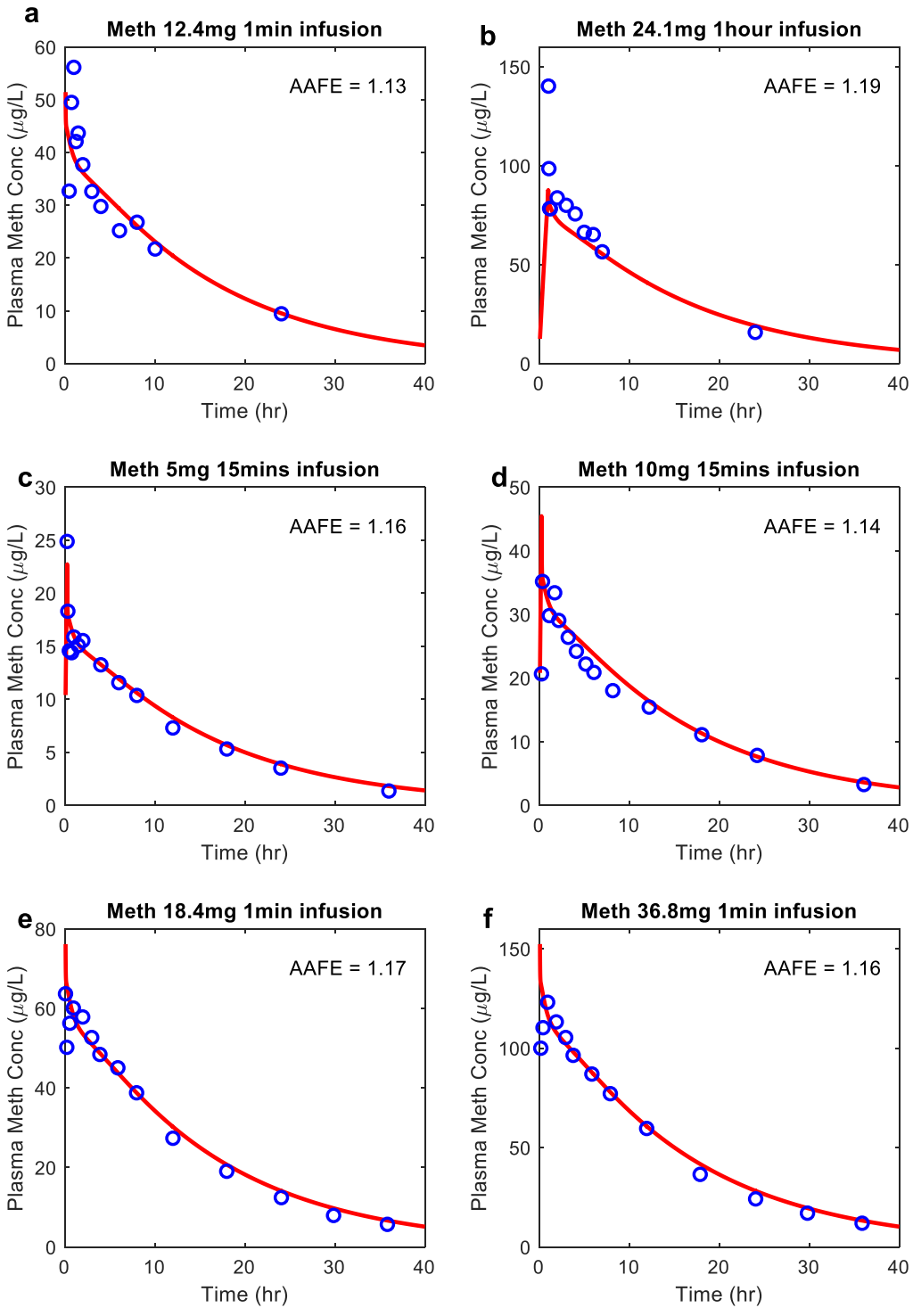

Figure 3.

JPET Fast Forward. Published on March 20, 2020 as DOI: 10.1124/jpet.120.264994
This article has not been copyedited and formatted. The final version may differ from this version.

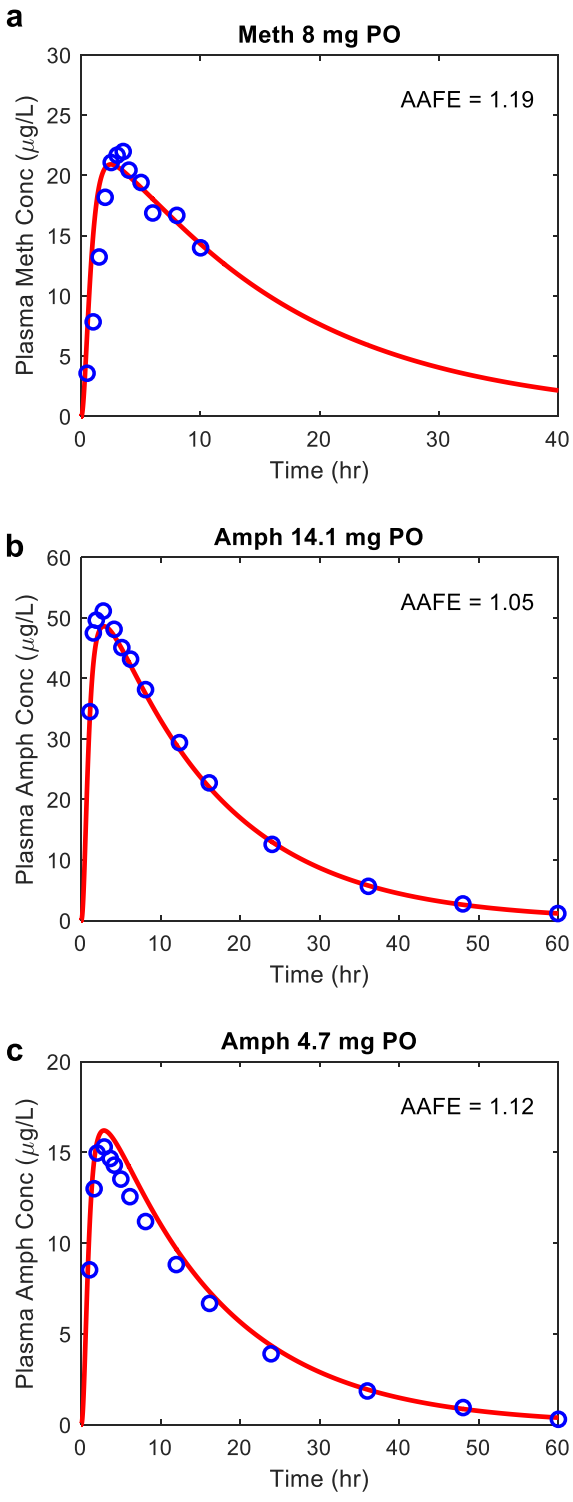

Figure 4.

JPET Fast Forward. Published on March 20, 2020 as DOI: 10.1124/jpet.120.264994
This article has not been copyedited and formatted. The final version may differ from this version.

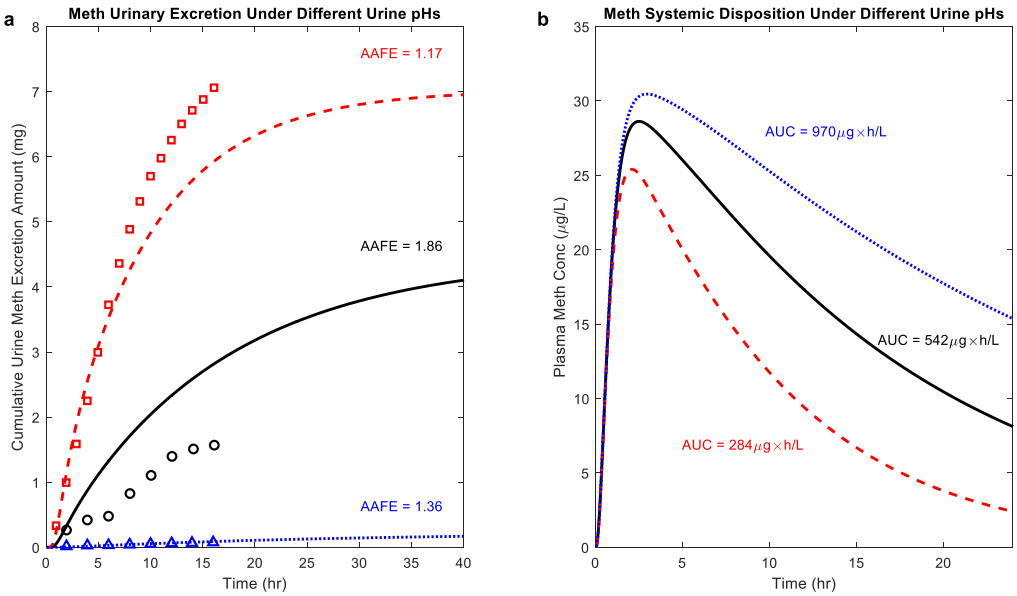

Figure 5.

JPET Fast Forward. Published on March 20, 2020 as DOI: 10.1124/jpet.120.264994
This article has not been copyedited and formatted. The final version may differ from this version.

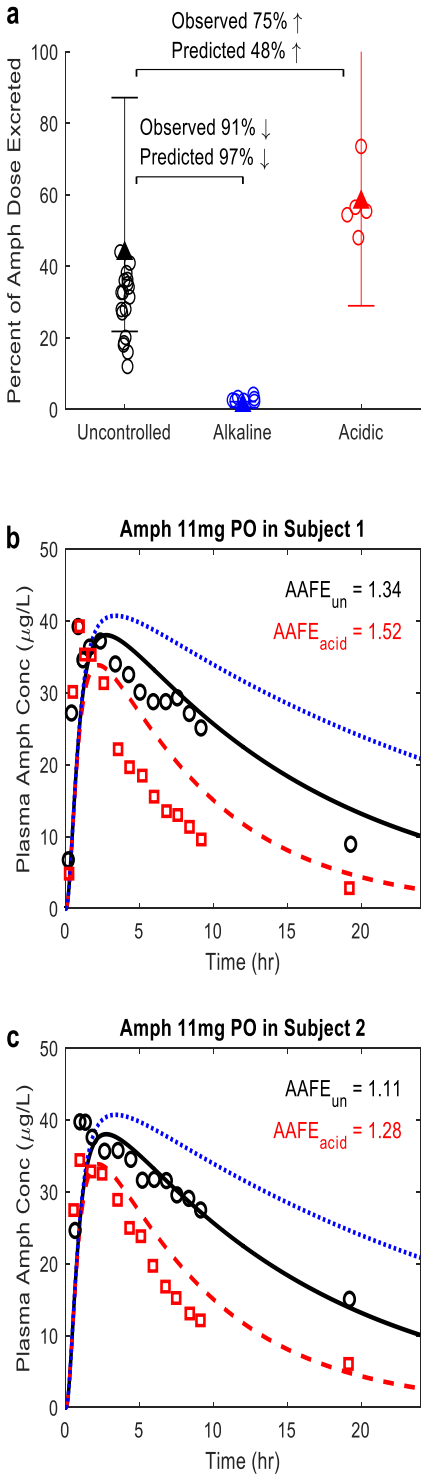

Figure 6.

JPET Fast Forward. Published on March 20, 2020 as DOI: 10.1124/jpet.120.264994
This article has not been copyedited and formatted. The final version may differ from this version.

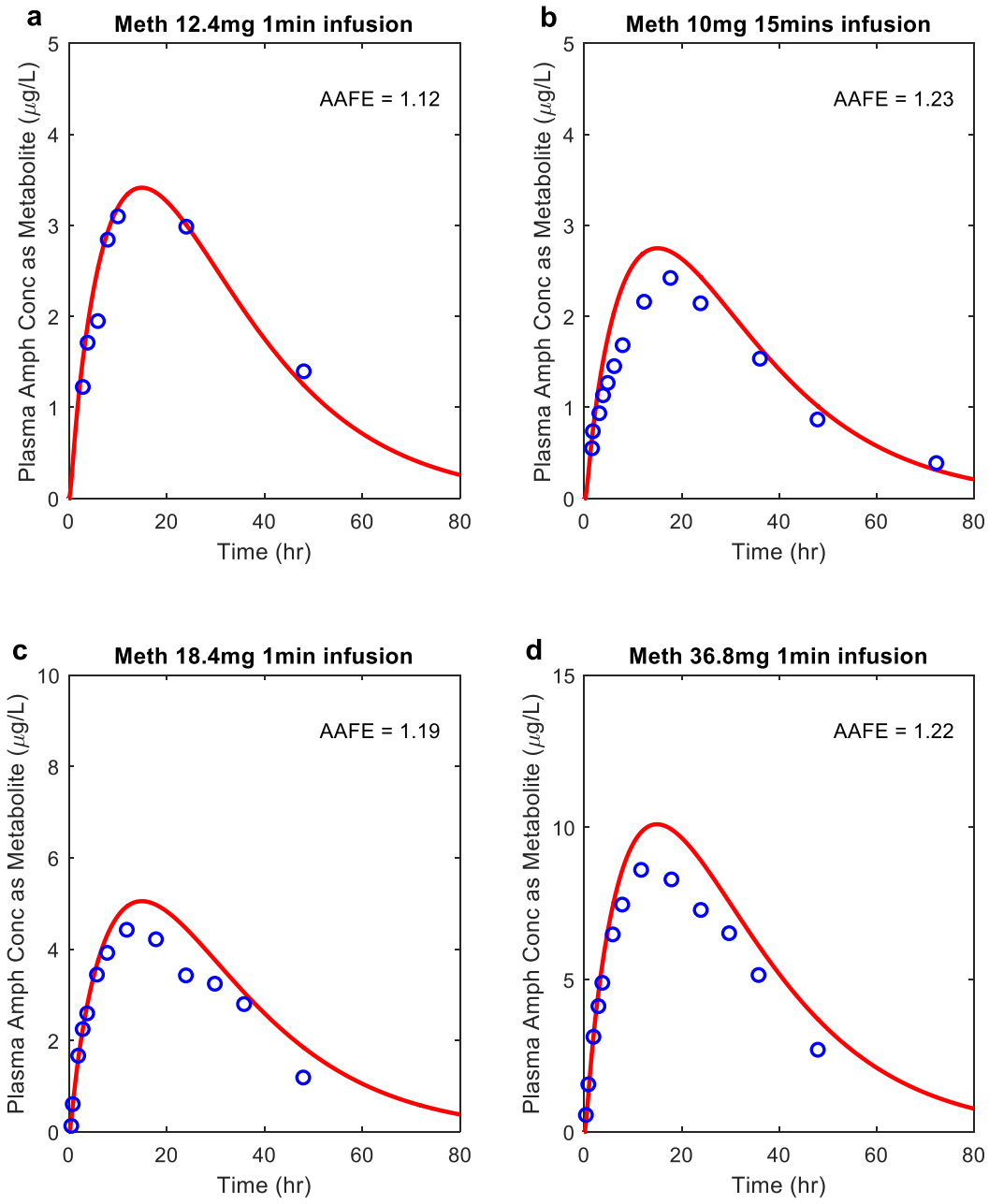

Figure 7.

JPET Fast Forward. Published on March 20, 2020 as DOI: 10.1124/jpet.120.264994
This article has not been copyedited and formatted. The final version may differ from this version.

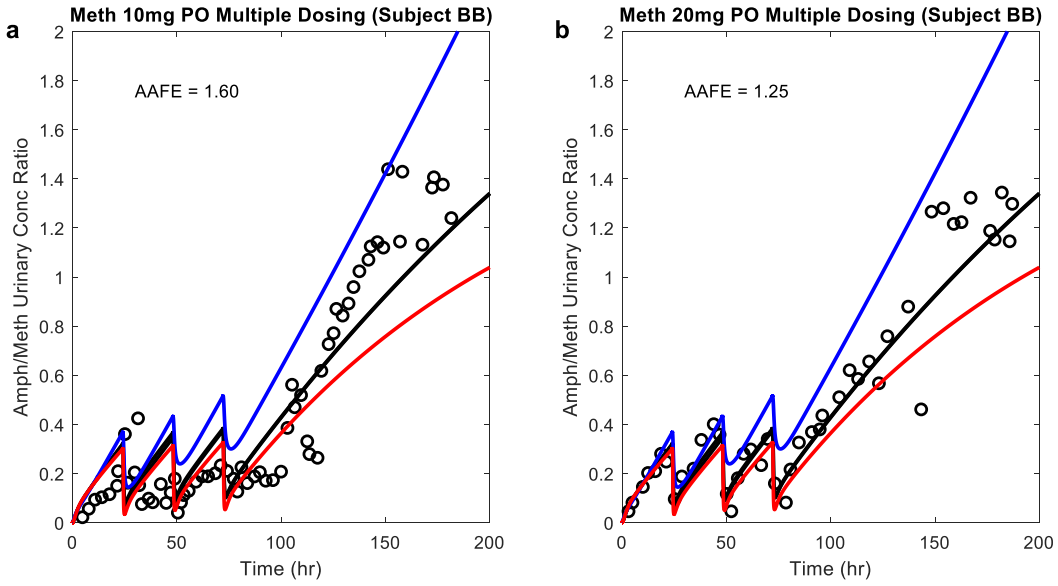

Figure 8.

JPET Fast Forward. Published on March 20, 2020 as DOI: 10.1124/jpet.120.264994
This article has not been copyedited and formatted. The final version may differ from this version.

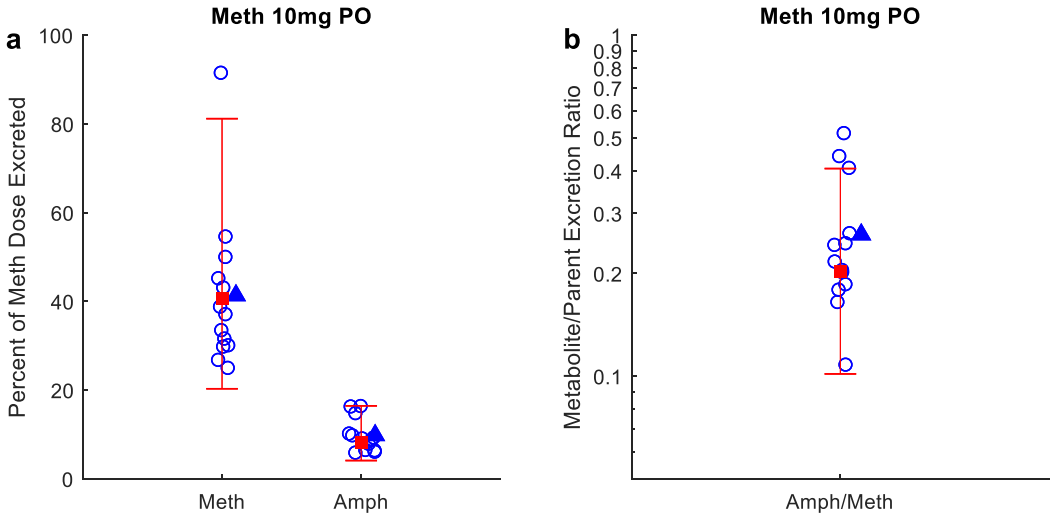

Figure 9.